Supporting information for: Evidence for Quantum Interference in SAMs of Arylethynylene Thiolates in Tunneling Junctions with Eutectic Ga-In (EGaIn) Top-Contacts

Davide Fracasso,[†] Hennie Valkenier,[†] J.C. Hummelen,[†] Gemma C. Solomon,[*,‡] and Ryan C. Chiechi[*,†]

Stratingh Institute for Chemistry and Zernike Institute for Advanced Materials, University of Groningen, Nijenborgh 4, 9747 AG Groningen, The Netherlands, and Nano-Science Center and Department of Chemistry, University of Copenhagen Universitetsparken 5, 2100 Copenhagen Ø, Denmark

E-mail: gsolomon@nano.ku.dk; r.c.chiechi@rug.nl

Experimental

Preparation of SAMs

Gold-on-mica substrates were prepared by thermally depositing the metal over a freshly cleaved mica substrates at 375 °C followed by cooling to room temperature *in vacuo* overnight. This procedure is known to give flat Au(111) substrates.[1,2] These substrates were immediately transferred to

[*]To whom correspondence should be addressed
[†]University of Groningen
[‡]University of Copenhagen

a nitrogen-filled glovebox. To form SAMs, first 0.5 mM solutions of the thioester precursors were prepared for AC, AQ, and AH in $CHCl_3$ and stirred at 50 °C for one hour. These solutions were filtered through 1 μm PTFE syringe filters[3] and combined with enough Et_3N to produce 10% (v/v) solutions. To ensure densely-packed SAMs, the freshly-prepared gold-on-mica substrates were immersed upside-down in these solutions for two nights. The samples were removed from solution, rinsed with $CHCl_3$, and then allowed to dry in the N_2 atmosphere of the glovebox. Immediately before measurement, each substrate was transferred from the glovebox to the EGaIn measurement setup. (Details about the use of Et_3N to prepare SAMs from thioesters are describe elsewhere.[4])

EGaIn Setup

The EGaIn setup itself is home-built, but inexpensive and simple, comprising a 10 μL glass syringe with a fixed, flat (*i.e.*, blunt), metal needle, mounted to a piezo-driven linear stepper (PI N-310.11) in open-loop mode controlled by a PI E-861 Nexact controller, a USB-powered CCD camera fitted with a variable-zoom telescopic lens (Edmund Optics, 600X magnification), and a source-meter with external current amplifier (Keithley 6430). The entire setup is enclosed in an Al box and rests on a thick piece of stone that dampens vibrations. The SAM is placed on an adjustable stage under the tip of the syringe and held in place with a spring-loaded ground-pin. The camera, piezo, and source-meter are connected to an external computer and controlled using LabView. The on-screen ruler used to measure the size of the junctions was calibrated using a micro ruler with 100 μm divisions.

Forming EGaIn Tips

Before beginning a measurement, a small drop of EGaIn (< 1 μL) is extruded such that it remains adhered to the end of the syringe needle. The drop is brought into contact with a sacrificial metal substrate (which can consist of a corner of the SAM being measured) and the syringe raised using the piezo (this step can be done by hand), forming and hourglass shape that cleaves in the center, leaving a tip attached to the syringe needle and a drop of EGaIn attached to the sacrificial substrate

(see Figure 2 for images of this process). The speed and the step-size affect the size and shape of the EGaIn tip, but the diameter of the tip is always $\sim 25\,\mu$m. In our hands, sharper tips not only allow the formation of smaller junctions, but enable the use of the same tip for multiple junctions, which speeds the acquisition of data (which is important for fragile SAMs); The more slowly the syringe is withdrawn, the sharper the EGaIn tips, thus the piezo affords control and reproducibility that cannot be achieved by hand. It is also important that there is a visible amount of EGaIn in the barrel of the syringe; as the syringe runs out, it becomes more difficult to produce long, sharp tips because the angle of the hourglass shape becomes more obtuse.

Data Acquisition

The current-amplifier of the source-meter is connected to the SAM via a triaxial cable; the positive terminal connects directly to the metal syringe needle, the negative pin to the SAM, and the ground-pin to Earth ground (see Supporting Information for a circuit diagram). The source-meter is also connected to Earth ground (as are all the metal parts of the EGaIn setup) which holds the Au substrate at ground; the bias is applied to the EGaIn. The camera is fixed on the EGaIn tip and the SAM is positioned underneath the tip manually using the adjustable stage. The source-meter is set at a fixed bias (typically 100 mV) and the tip slowly brought into contact with the SAM using the piezo to form a junction. When the current exceeds the "no-contact" value ($\sim$ 5 pA) the piezo is stopped and the current is measured for 20 s; if it remains stable, then a fast I/V sweep is performed, and the tip is either lowered another increment (the speed and distance of which are determined by the SAM and the experience of the operator) or, if a short is found, moved to another location. This process is repeated sequentially until the data transition from no-contact traces to either a shorted or non-shorted trace. When a non-shorted junction occurs ($\sim$ 80% of junctions) the diameter of the junction is measured on-screen and five J/V traces are recorded where one J/V trace is: 0 V $\rightarrow +V_{max} \rightarrow -V_{max} \rightarrow$ 0 V. (These traces comprise the raw data set.) Although the actual contact is likely smaller than the measured area, this discrepancy is systematic and therefore not corrected for. During the five traces a junction can short or revert to a no-contact

trace. We, and others,[5] have observed that the experience of the operator impacts the precision of the measurement, but we have not been able to quantify the effect; a less experienced operator would likely encounter a lower yield of non-shorted junctions and more broadly-distributed data.

Data Processing

All of the software is homemade using SciPy Python bindings, BASH, and the GnuPlot plotting utility, all of which are open-source and freely-available. The raw data, consisting of five J/V traces each of many junctions across several substrates, are filtered through an algorithm that prunes the no-contact traces and shorts by line-shape and magnitude (see Supporting Information for examples of raw and pruned data sets). The values of J are aligned to their corresponding values of V and the geometric average of J, $\bar{J}$, arithmetic average of the rectification ratios, $\bar{R}$, and histograms (bin size = 150) of $log|J|$ for each value of V along with the standard error of the mean, SE_m, are computed. The histograms are automatically fit to the Gaussian function, $f(V)$, using the least-squares fitting routine from GnuPlot, which reports the mean, μ_{log}, variance, σ^2_{log}, and SE_m of μ_{log} and σ_{log} without human involvement, though the fits are visually inspected after the fact. This method produces larger standard deviations, σ_{log}, than manual fits (*e.g.*, using Origin), but removes the expectation bias and arguably artificially low σ_{log} that can result from fits using a GUI-driven interface on these types of data sets. (The specific equations used are listed below.)

Measurement and Data Processing Details

EGaIn Measurements

All electrical measurements were performed using a Keithley 6430 sub-femto source-meter with the bundled pre-amp wired according to Figure 1. All measurements were performed in an Al box that serves as a Faraday cage. The junctions were imaged using a halogen light and a zoom lens/CCD camera (Edmund Optics). Although no differences between the data measured under

illumination and in the dark were found, all measurements were performed in the dark and the duration and intensity of the light used to position the EGaIn tip was kept to a minimum.

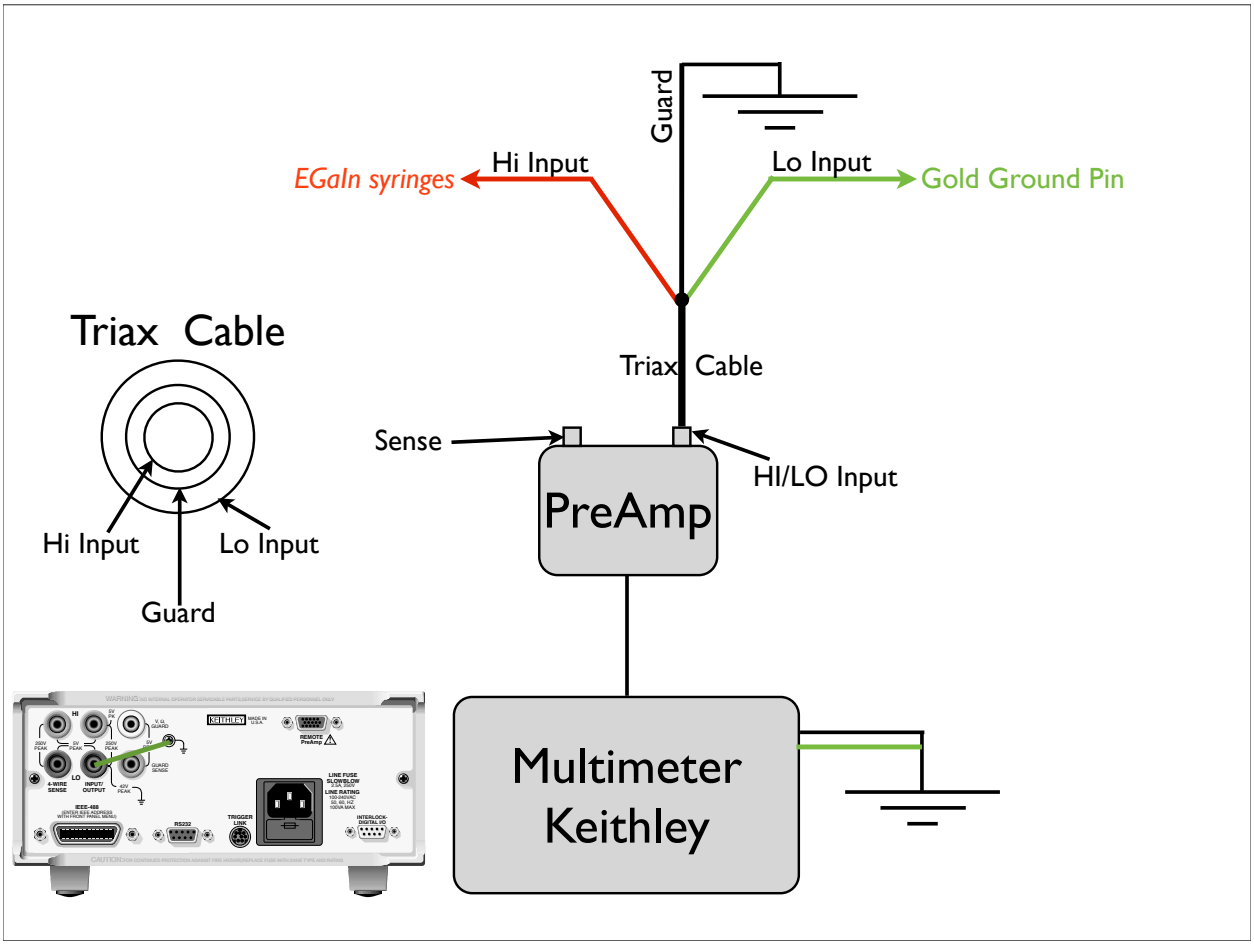

Figure 1: Wiring diagram for the connection of the source-meter to the EGaIn drop. The Lo Input is bridged to the ground at the meter, which references the Lo Input from the PreAmp to ground as well.

EGaIn tips were formed by extruding a small drop of EGaIn (< 1 μL) such that it remains adhered to the end of the syringe needle. The drop was stuck to a sacrificial metal substrate and the syringe raised either using the piezo or by hand. The diameter of the tip is influenced by the speed of withdraw (slower speeds lead to smaller tips). The length of the tip (*i.e.*, from the end of the needle to the tip of the EGaIn) is influenced by the amount of EGaIn in the barrel of the syringe; below a threshold amount (approximately when there is no EGaIn visible in the syringe) the length of the tip decreases. Figure 2 shows sequential images of the formation of a tip.

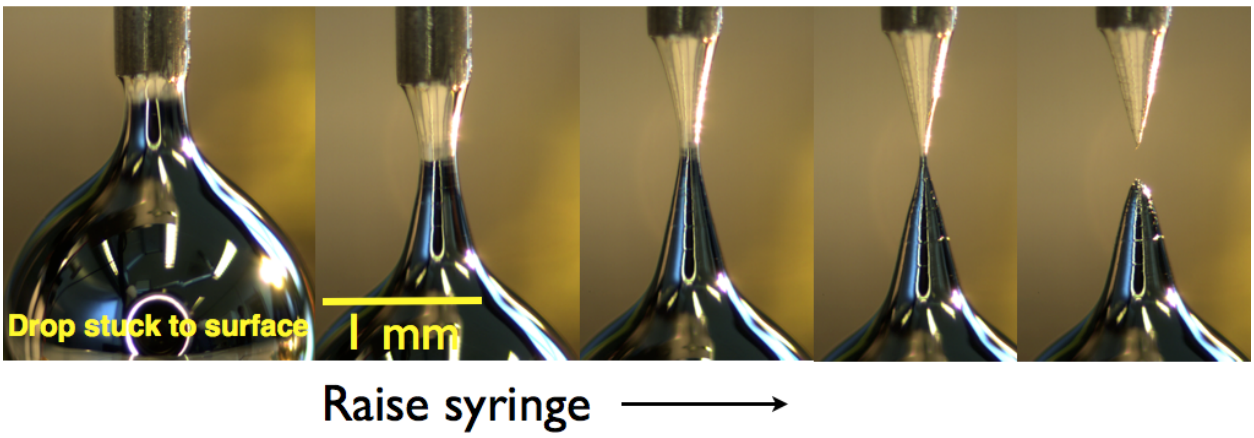

Figure 2: Sequential images of the formation of an EGaIn tip. First, a drop is stuck to a sacrificial substrate, then the syringe is raised slowly, forming an hourglass shape. At a certain point the hourglass shape severs at the thinnest point, leaving behind an EGaIn tip and a drop that is discarded. The difference in color between the top and bottom of the hourglass shapes is from the reflection of the gold surface.

Data Processing

The raw data, comprising five scans per junction, were filtered through a pruning algorithm (written in Python using the SciPy package) to remove shorted traces, no-contact traces, and other anomalous traces. An example from one AC substrate is shown in Figure 3. The algorithm separates the data into individual traces comprising one sweep: 0 V $\rightarrow +V_{max} \rightarrow -V_{max} \rightarrow$ 0 V. The traces are filtered by defining shorts as I/V curves where $I > 10$ mA ($J \approx 10^3$ A/cm^2) at 0.2 V and no-contact traces where $J \neq 0$ at 0 V, or in which dI/dV changes sign five or more times during a forward or reverse trace (*i.e.*, the trace is noisy). A trace that shorts or converts to no-contact at any point is entirely discarded (which is why some traces above the threshold appear to be pruned in Figure 3.)

These pruned data were then separated by sorting the value of J at each V for every trace, the geometric-average was calculated (Eq. (1)), the average rectification ratio (Eq. (2)), and then a histogram of J was constructed for each V. The geometric-averaged values of J were plotted using the standard error of the mean (Eq. (3)) as error bars. Each histogram was fitted to a Gaussian function (Eq. (4)) using the least squares fitting routine of GnuPlot. The mean value of each Gaussian fit was then plotted against V. Examples of the histograms for AC, AQ, and AH comprising 218, 268, and 232 traces respectively are pictured in Figure 4. Histograms for AC including the additional

two substrates (782 traces total) are pictured in Figure 5. The cropping of the data at $J \approx 1$ A/cm^2 are particularly obvious in Figure 4b, Figure 4d, Figure 5b, and Figure 5d.

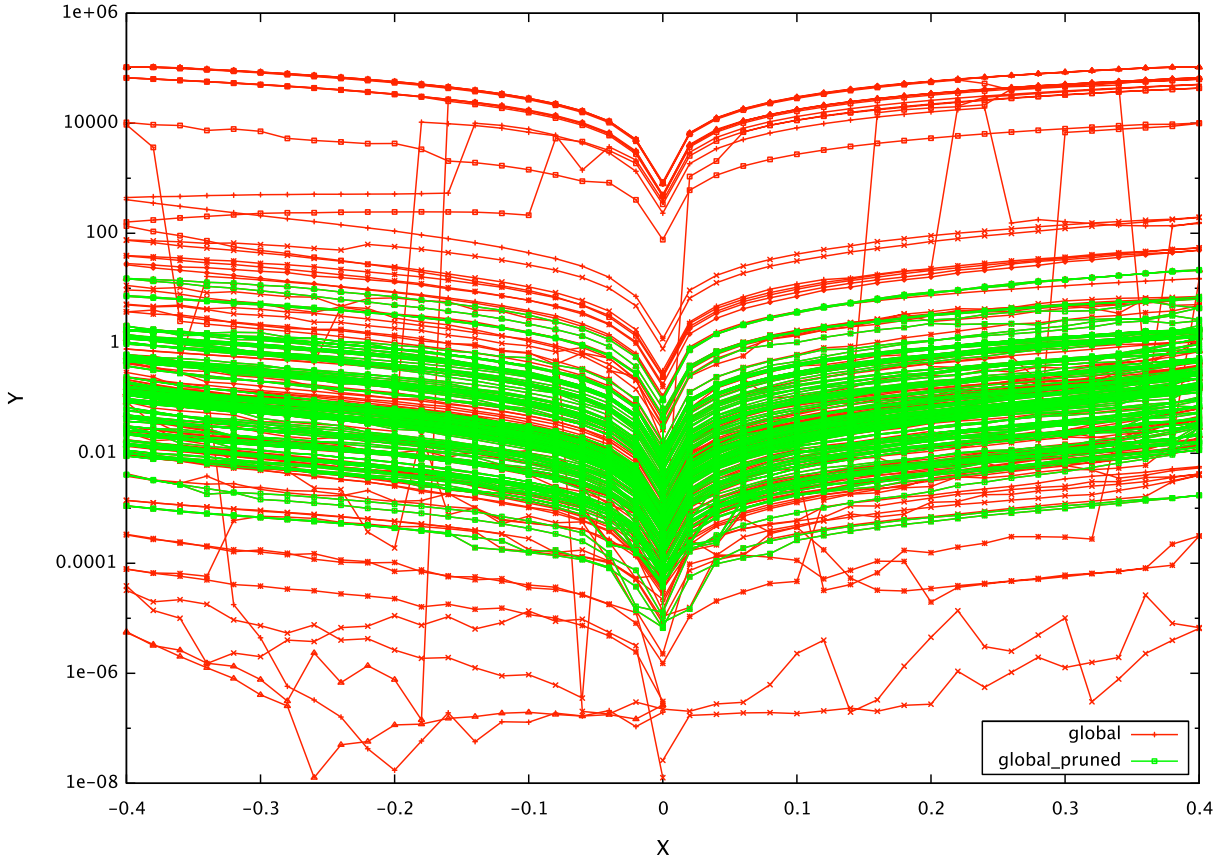

Figure 3: A plot of the raw data from one AC substrate showing the raw data (global, red) and the data after pruning the data using a custom algorithm (global_pruned, green). The X and Y axes are Potential (V) and Current-Density (A/cm^2) respectively.

$$\bar{J} = (\prod_{i=1}^{n} J_i)^{\frac{1}{n}} \tag{1}$$

$$\bar{R} = \frac{\sum_{i=1}^{n} R_i}{n}, \quad R = \frac{J(+V)}{J(-V)}, \quad R_i = \frac{|J_{i+}|}{|J_i|} \tag{2}$$

$$SE_m = \frac{s}{\sqrt{n}}, \quad s = \sqrt{\frac{1}{n-1}\sum_{i=n}^{n}(J_i - \bar{J})^2} \tag{3}$$

$$f(V) = \frac{1}{\sqrt{2\pi\sigma^2}} e^{-\frac{(V-\mu)^2}{2\sigma^2}} \tag{4}$$

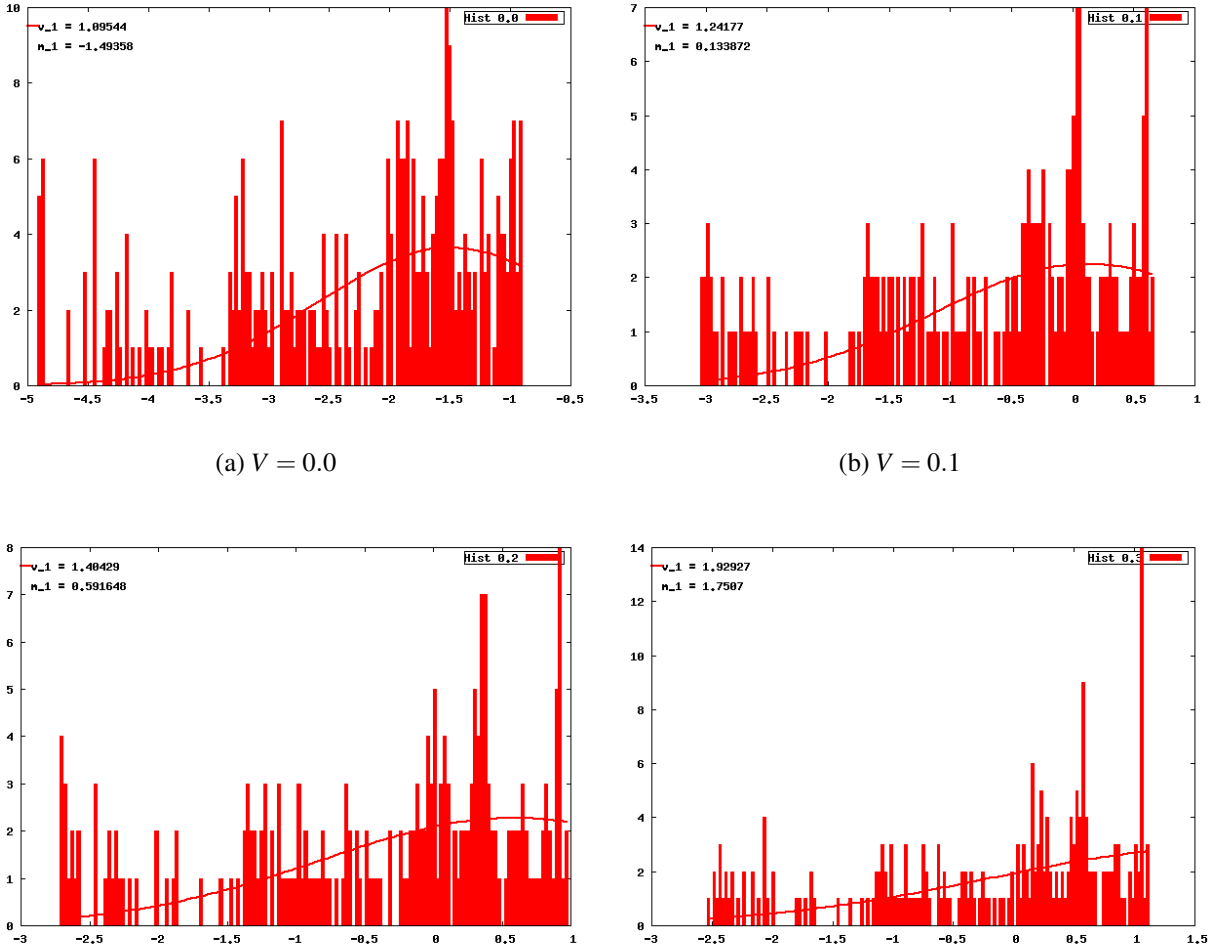

(a) $V = 0.0$ (b) $V = 0.1$

(c) $V = 0.2$ (d) $V = 0.3$

Figure 4: Histograms of AC for $V = 0.0, 0.1, 0.2,$ and 0.3 V.

The histograms reported in the main text are re-plotted from the fits shown in Figure 6. Since the height of a Gaussian is not affected by the fitting parameters, we normalize the histograms and the fits to 1 and plotted them from $log|J| = -4 - +4$ for clarity.

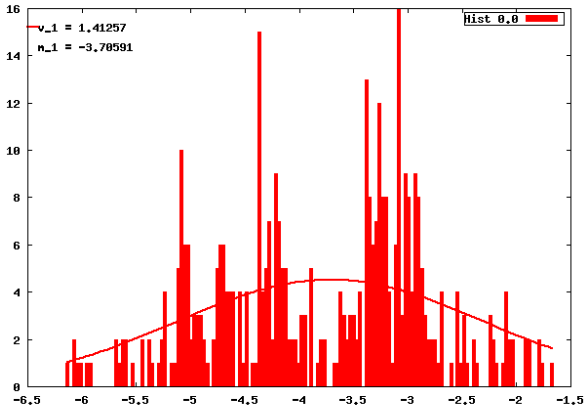

(e) $V = 0.0$

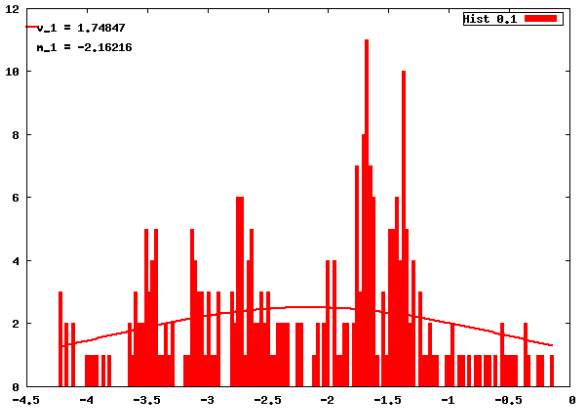

(f) $V = 0.1$

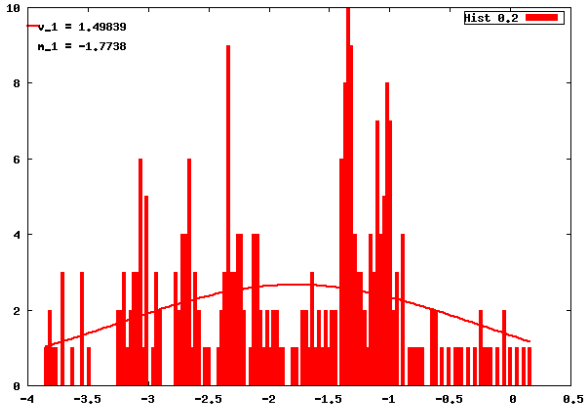

(g) $V = 0.2$

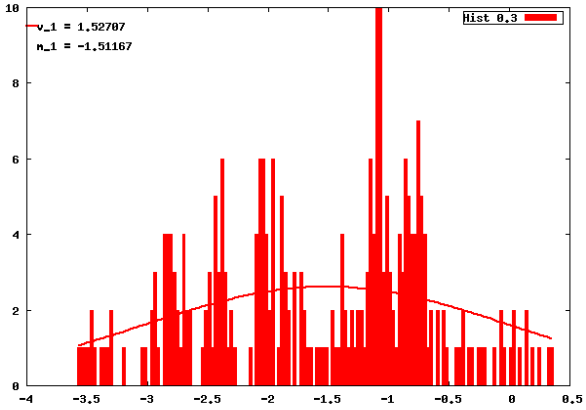

(h) $V = 0.3$

Figure 4: Histograms of AQ for $V = 0.0, 0.1, 0.2,$ and 0.3 V.

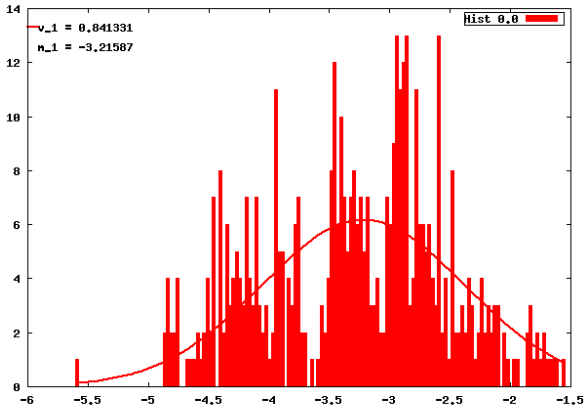

(i) $V = 0.0$

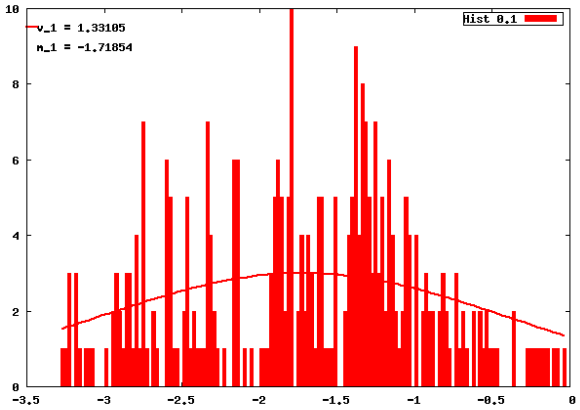

(j) $V = 0.1$

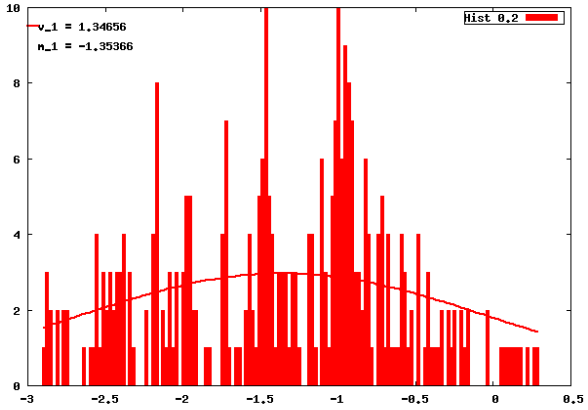

(k) $V = 0.2$

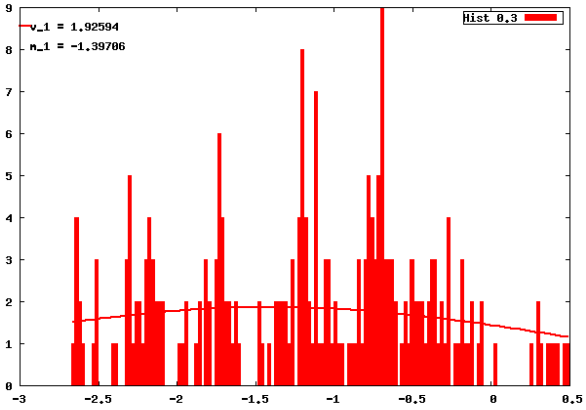

(l) $V = 0.3$

Figure 4: Histograms of AH for $V = 0.0, 0.1, 0.2,$ and 0.3 V.

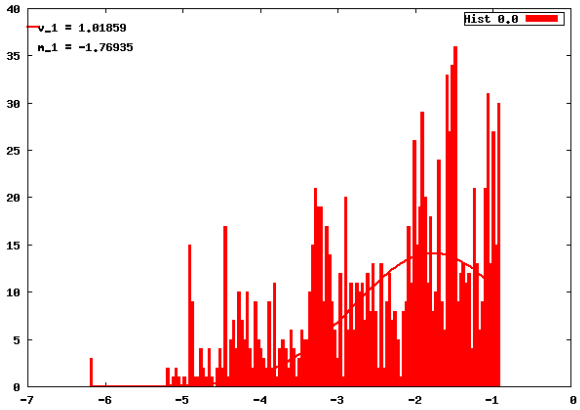

(a) $V = 0.0$

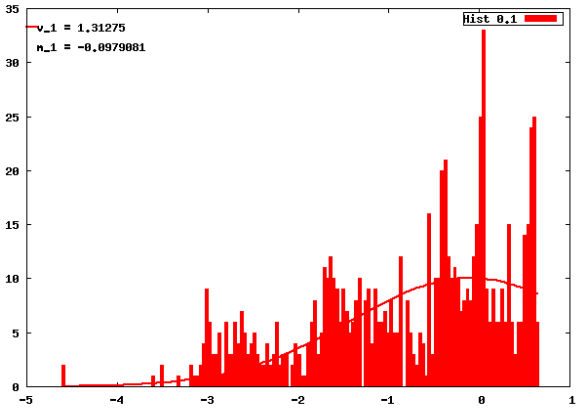

(b) $V = 0.1$

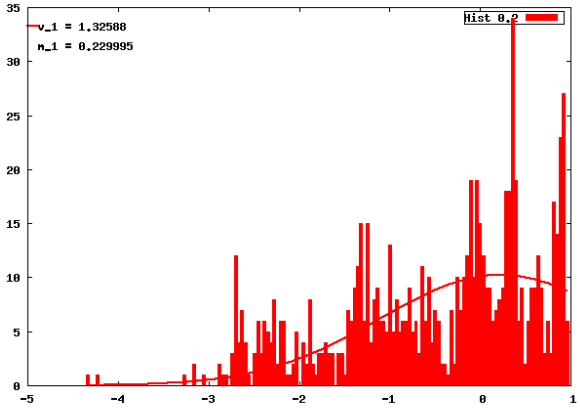

(c) $V = 0.2$

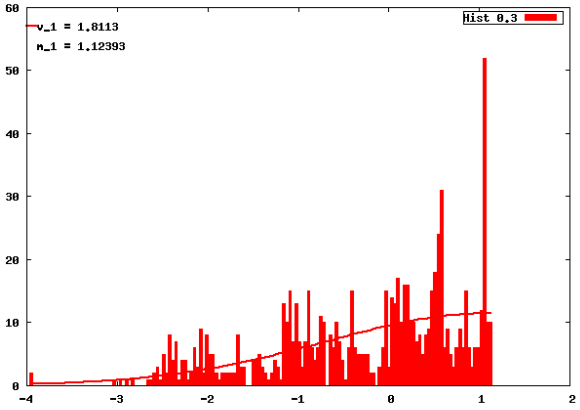

(d) $V = 0.3$

Figure 5: Histograms of AC for $V = 0.0, 0.1, 0.2,$ and 0.3 V including the additional two substrates.

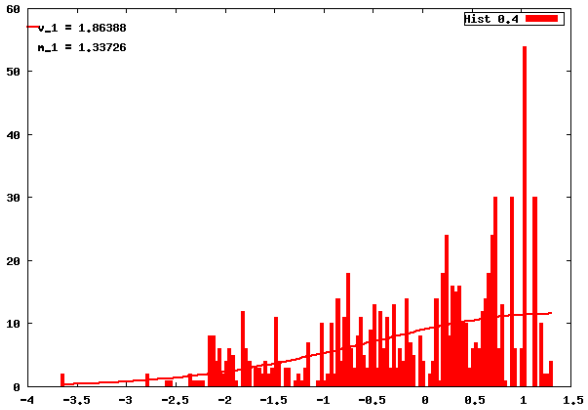

(a) AC @ $V = 0.4$

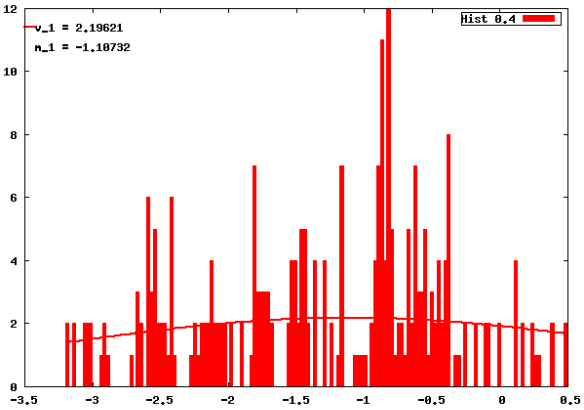

(b) AQ @ $V = 0.4$

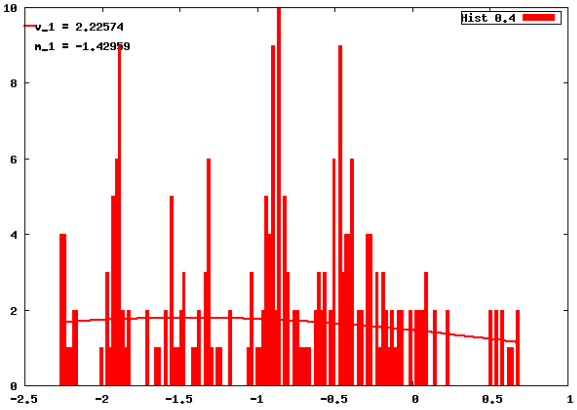

(c) AH @ $V = 0.4$

Figure 6: Histograms of AC, AQ, and AH at $V = 0.4$ V as output by the fitting program; these data are replotted in the main text and normalized to 1.

Self-Assembled Monolayers

The thicknesses of the SAMs of AC, AQ, and AH were measured using a combination of ellipsometry and XPS. The interpretation of these data is discussed in detail elsewhere.[6] Briefly; due to differences in the dielectric constants, absorption spectra, and elemental composition of AC, AQ, and AH, we combined ellipsometry with two separate methods of determining thicknesses by XPS.[7,8] We weighted each method according to how reliable it was for each of the three SAMs. These data are summarized in Table 1 along with the weights assigned to each method in parentheses. The difference in energies between linear AH (24.62 Å) and AH with a 30° bend (23.80 Å) are negligible (2.08 kcal/mol), thus we do not know which form is adopted in the SAM. This bend causes a 0.88 Å difference in the calculated length and therefore is not enough to account for the apparent decrease in the measured thickness, which may be due to differences in the optical properties induced by the broken conjugation (*e.g.*, ellipsometry is very sensitive to changes in dielectric constant). Nonetheless, we cannot rule out the possibility that SAMs of AH are ~ 5 Å thinner than SAMs of AC and AQ.

Table 1: Calculated and Measured Lengths/Thicknesses (Å); weights are shown in parentheses.

	DFT[a] Length	**Ellipsometric Thickness**	**XPS Thickness[b]**	**XPS Thickness[c]**	**Weighted Average**
AC	24.52	28.6 (0)	24.1 (2)	27.1 (1)	25.1
AQ	24.52	21.7 (1)	20.1 (0)	26.9 (1)	24.3
AH	24.62	19.1 (3)	18.3 (2)	20.1 (1)	19.0

[a] B3LYP/6-311g** geometry optimization

[b] Calculated from the C:Au ratio

[c] Calculated from the attenuation of the Au signal

Bibliography

The full list of authors for reference "Shao, Y. et al. *PCCP* **2006**, *8*, 3172–3191" is: Shao, Yihan and Molnar, Laszlo Fusti and Jung, Yousung and Kussmann, Jorg and Ochsenfeld, Christian and Brown, Shawn T. and Gilbert, Andrew T. B. and Slipchenko, Lyudmila V. and Levchenko,

Sergey V. and O'Neill, Darragh P. and Jr, Robert A. DiStasio and Lochan, Rohini C. and Wang, Tao and Beran, Gregory J. O. and Besley, Nicholas A. and Herbert, John M. and Lin, Ching Yeh and Voorhis, Troy Van and Chien, Siu Hung and Sodt, Alex and Steele, Ryan P. and Rassolov, Vitaly A. and Maslen, Paul E. and Korambath, Prakashan P. and Adamson, Ross D. and Austin, Brian and Baker, Jon and Byrd, Edward F. C. and Dachsel, Holger and Doerksen, Robert J. and Dreuw, Andreas and Dunietz, Barry D. and Dutoi, Anthony D. and Furlani, Thomas R. and Gwaltney, Steven R. and Heyden, Andreas and Hirata, So and Hsu, Chao-Ping and Kedziora, Gary and Khalliulin, Rustam Z. and Klunzinger, Phil and Lee, Aaron M. and Lee, Michael S. and Liang, WanZhen and Lotan, Itay and Nair, Nikhil and Peters, Baron and Proynov, Emil I. and Pieniazek, Piotr A. and Rhee, Young Min and Ritchie, Jim and Rosta, Edina and Sherrill, C. David and Simmonett, Andrew C. and Subotnik, Joseph E. and Iii, H. Lee Woodcock and Zhang, Weimin and Bell, Alexis T. and Chakraborty, Arup K.

Notes and References

(1) DeRose, J. A.; Thundat, T.; Nagahara, L. A.; Lindsay, S. M. *Surf. Sci.* **1991**, *256*, 102–108.

(2) Porath, D.; Goldstein, Y.; Grayevsky, A.; Millo, O. *Surface Science* **1994**, *321*, 81 – 88.

(3) Filtration is not necessary for solutions of $CHCl_3$, but we observed some precipitates in previous experiments using THF with AC and AQ.

(4) Valkenier, H.; Huisman, E. H.; van Hal, P. A.; de Leeuw, D. M.; Chiechi, R. C.; Hummelen, J. C. *Journal of the American Chemical Society* **2011**, *133*, 4930–4939.

(5) Thuo, M. M.; Reus, W. F.; Nijhuis, C. A.; Barber, J. R.; Kim, C.; Schulz, M. D.; Whitesides, G. M. *J. Am. Chem. Soc.* **2011**, *133*, 2962–2975.

(6) Valkenier, H.; Guédon, C.; Markussen, T.; Thygesen, K.; van der Molen, S. J.; Hummelen, J. C. Manuscript in preparation.

(7) Thome, J.; Himmelhaus, M.; Zharnikov, M.; Grunze, M. *Langmuir* **1998**, *14*, 7435–7449.

(8) Bain, C. D.; Whitesides, G. M. *The Journal of Physical Chemistry* **1989**, *93*, 1670–1673.